Geophysical Research Letters

RESEARCH LETTER
10.1029/2025GL116437

The Latent Heating Feedback on the Mid-Latitude Circulation

Henrik Auestad[1], **Abel Shibu**[2], **Paulo Ceppi**[2], **and Tim Woollings**[1]

[1]Atmospheric, Oceanic and Planetary Physics, University of Oxford, Oxford, UK, [2]Department of Physics, Imperial College London, London, UK

Key Points:

- The latent heating feedback strengthens the subtropical jet and shifts the nearby storm track equatorward
- Where the subtropical jet is weak, the latent heating feedback enhances the poleward propagation of storms and the jet tilt
- The responses follow from the latent heating feedback on synoptic scales and subsequently the distribution of baroclinicity

Supporting Information:

Supporting Information may be found in the online version of this article.

Correspondence to:

H. Auestad,
henrik.auestad@physics.ox.ac.uk

Citation:

Auestad, H., Shibu, A., Ceppi, P., & Woollings, T. (2025). The latent heating feedback on the mid-latitude circulation. *Geophysical Research Letters*, *52*, e2025GL116437. https://doi.org/10.1029/2025GL116437

Received 8 APR 2025
Accepted 24 AUG 2025

Author Contributions:

Conceptualization: Henrik Auestad, Paulo Ceppi, Tim Woollings
Data curation: Henrik Auestad, Abel Shibu
Formal analysis: Henrik Auestad, Paulo Ceppi, Tim Woollings
Funding acquisition: Tim Woollings
Investigation: Henrik Auestad
Methodology: Henrik Auestad, Paulo Ceppi, Tim Woollings
Resources: Tim Woollings
Software: Henrik Auestad, Abel Shibu
Supervision: Paulo Ceppi
Validation: Henrik Auestad
Visualization: Henrik Auestad
Writing – original draft: Henrik Auestad

Abstract Midlatitude storms transport warm and moist air poleward and upward, releasing latent heat. Latent heating is thus organized by the circulation but then modifies temperature gradients and winds, constituting a nonlinear feedback. We define the latent heating feedback as the effects that arise from latent heating being coupled with the circulation. Because of its nonlinearity, the climatic effects of this feedback are difficult to isolate and remain poorly understood. By decoupling latent heating from the circulation in an atmospheric general circulation model, we show that the latent heating feedback enhances storm track eddy diffusivity, modifying eddy heat fluxes beyond changes in mean baroclinicity. Simultaneously, tracked storms occur at lower latitudes, intensify more, and propagate further poleward, while the subtropical jet strengthens as coupled latent heating preserves lower latitude baroclinicity. The feedback response supports the idea that diabatic effects cause the "too zonal, too equatorward" storm track biases in climate models.

Plain Language Summary Midlatitude storms transport water vapor poleward and upward. When ascending, the air cools, causing the vapor to condense, releasing latent heat. The latent heating boosts the ascent in which it occurs and amplifies the storms originally responsible for the heating. This circular chain of events couples latent heating and storms in a nonlinear relationship we call the *latent heating feedback*. We simulate an atmosphere where latent heating is static and not a consequence of warm, moist air ascending. Comparing this to an atmosphere with realistic latent heating, we show that realistic latent heating leads to more intense storms traveling further poleward, especially west of North America and Europe. Simultaneously, the longitudinally averaged jet streams and storms respond by retracting toward the equator, leaving reduced westerlies and a double jet tendency over North America and Europe. Previous works tend to focus on the effect of latent heating on the average atmospheric state. Our work shows that this effect is only part of the story and that the latent heating effect on storms directly causes regional differences that climate models struggle with.

1. Introduction

The time mean latent heating in the midlatitude storm tracks forces a zonally varying mean state both forcing and interacting with the stationary wave pattern (Held et al., 2002; Kaspi & Schneider, 2013). However, storm-track latent heating is not static but occurs in poleward moving and ascending warm and moist air masses (Auestad et al., 2024; Pauluis et al., 2010). Thus, condensation is organized by the dynamics and the consequential latent heat release feeds back on the dynamics by enhancing ascent and modifying temperature gradients. We here define the specific impact of latent heating being coupled with the dynamics, as distinct from a static time-mean forcing mimicking latent heating, the *latent heating feedback*.

On synoptic and shorter time scales, in the lower troposphere, latent heating enhances the ascent in which it occurs and modifies static stability leading to stronger and smaller cyclones (Booth et al., 2013; Emanuel et al., 1987; O'Gorman, 2011; Tierney et al., 2018). In the upper troposphere, latent heating sharpens potential vorticity (PV) gradients and jets (Bukenberger et al., 2023; Harvey et al., 2020) and enhances the vertical advection of low PV air, amplifying negative upper tropospheric PV anomalies (Madonna, Wernli, et al., 2014; Methven, 2015) that may promote anticyclonic Rossby wave breaking (Madonna, Limbach, et al., 2014; Zhang & Wang, 2018) and maintain blocks (Pfahl et al., 2015).

Of relevance for time scales beyond synoptic, Hoskins and Valdes (1990) suggested that latent heating maintains baroclinicity, energizing the storm track. The effect of latent heating on baroclinicity has since been debated (Laîné et al., 2011; Papritz & Spengler, 2015; White et al., 2024; Woollings et al., 2016; Xia & Chang, 2014) and some differences stem from the spatio-temporal resolution of latent heating and winds used to analyze this effect

Writing – review & editing: Henrik Auestad, Paulo Ceppi, Tim Woollings

(Auestad et al., 2024): instantaneous data indicate that latent heating strengthens baroclinicity, while spatio-temporally averaged data suggest a weakening.

This paper aims to demonstrate the existence of the latent heating feedback and understand how it influences the jet and storm track on climatic time scales. Due to its nonlinearities, it is difficult to examine the latent heating feedback in isolation in integrated climate simulations. Schemm (2023) suggested that a realistic representation of latent heating is important for capturing the climatological storm track tilt downstream of a sea surface temperature (SST) front, consistent with how latent heating is expected to enhance the poleward propagation of cyclones (Tamarin & Kaspi, 2016). Hermoso et al. (2024) showed that increasing latent heating shifted the jet poleward over the Gulf Stream extension in reanalysis from 1979 to 2022, while simultaneously leading to an equatorward shift downstream via its effect on eddy momentum fluxes, suggesting that the effects are regional.

To examine the regional climatic effects of the latent heating feedback in isolation, we introduce an experimental design where latent heating is decoupled from the dynamics only in the extratropics. We show that the latent heating feedback strengthens the subtropical jet in a zonally symmetric fashion. At the same time, cyclones grow faster and stronger and propagate more poleward in regions of a weak subtropical jet. In these regions, the polar jet is strengthened, causing a more tilted storm track and jet.

2. Methods

2.1. Model

We run the Community Atmosphere Model 4.0 (CAM4), an atmospheric model component of the Community Earth System Model (Neale et al., 2013), with topography and seasonally varying prescribed climatological sea surface temperatures from the period 1995–2005 (Hurrell et al., 2008). The model uses the finite volume method and has a 0.9-degree meridional grid spacing, a 1.25-degree zonal grid spacing and 26 vertical levels. Using ARCHER2 (Beckett et al., 2024), we run the experiments for 50 years, following 1 year of spin-up that is discarded.

2.1.1. Experimental Setup

To examine the latent heating feedback, we run a model experiment where the latent heating is decoupled from the dynamics. The temperature tendencies produced by the CAM4 shallow convection scheme (Hack, 1994), deep convection scheme (Zhang & McFarlane, 1995), and the micro-physics scheme (Rasch & Kristjánsson, 1998) constitute the temperature tendencies due to condensation and evaporation. This temperature tendency, referred to as *latent heating*, includes condensation due to resolved and parametrized convection and can be negative due to evaporation (Figure 1). While decoupling latent heating, the other diabatic tendencies (e.g., radiation) are left to evolve freely. Decoupling latent heating causes some changes in the other diabatic terms, which contribute to the zonal mean temperature budget (following Lachmy & Kaspi, 2020, see Figures S5 and S6 in Supporting Information S1).

We decouple latent heating by replacing the real-time latent heating with the monthly mean latent heating in the control run, analogous to prescribing SST. The mean latent heating is calculated and prescribed at every individual grid point on model levels (sigma-hybrid). The prescribed latent heating follows the seasonal cycle, so the climatological January latent heating in the control run is prescribed to January in the decoupled run (Figures 1b and 1c).

To minimize the effect of decoupling on the Hadley circulation, latent heating is only prescribed outside of the tropics. We define the tropics as where the 200 hPa control run eddy kinetic energy (EKE) is smaller than the respective hemispheric median EKE. EKE is given by $(1/2)\left(u'^2 + v'^2\right)$, where the primes denote high pass filtered 6-hourly values with a 10-day cut-off period, using a 243 point Lanczos filter (Duchon, 1979). Before calculating the tropical-extratropical boundaries, we smooth the EKE by applying a three-month running mean and a 21-grid point running mean, the latter on both the meridional and zonal dimensions. The calculations are done for each month, such that the boundaries follow a seasonal cycle. This is a pragmatic definition of the tropics that allows for only decoupling latent heating where extratropical cyclones exist climatologically. The dashed lines in Figures 1a and 1b show these boundaries for January.

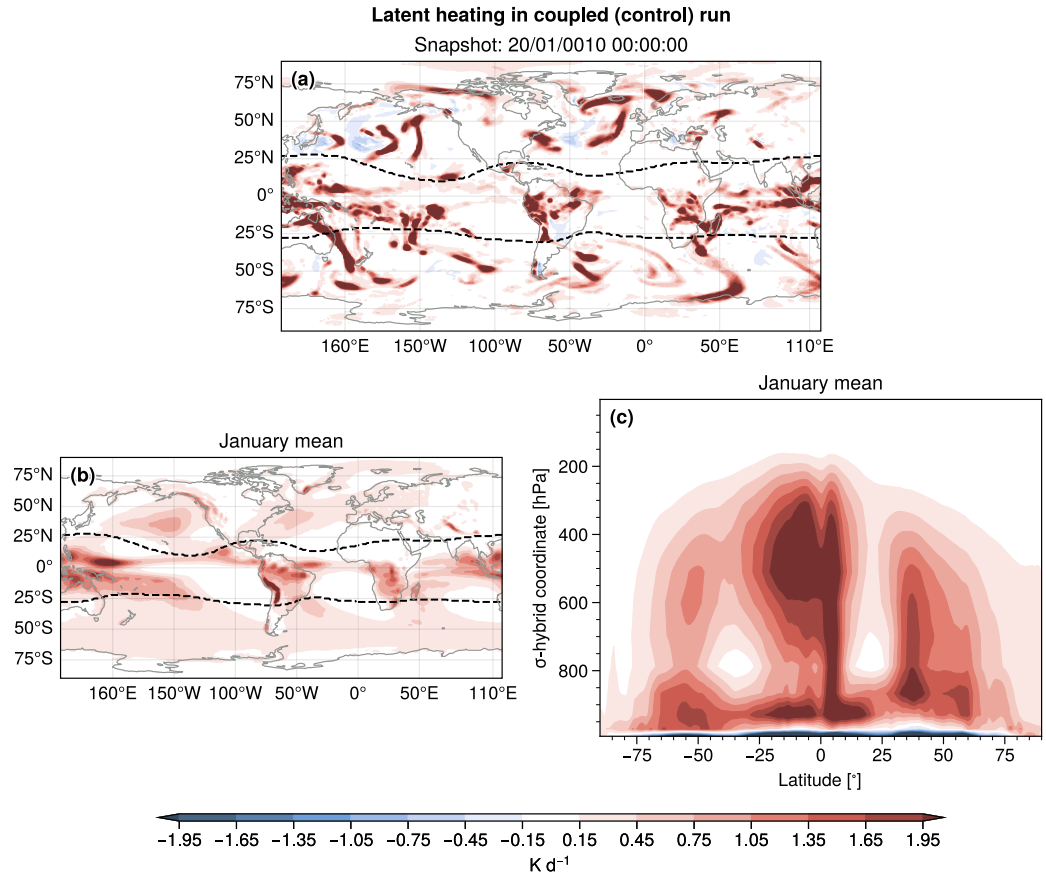

Figure 1. Latent heating in the coupled (control) run for a snapshot in time (a) and the January average (b, c). Using all model levels, the unweighted vertical average latent heating is shown in panels (a, b) and the zonally average is shown in panel (c). The black dashed lines (a, b) show the tropical-extratropical boundaries defined in the text. The colorbar refers to all panels.

Additionally, the decoupling is only applied above the boundary layer, reading the boundary layer height at every time step. Boundary layer processes involve a mixture of sensible and latent heating, as well as cooling by evaporation (Figure 1c). Fixing the latent heat exchange disturbs the energy balance in the boundary layer mixing processes, which we thus avoid. However, we also performed decoupled simulations where extratropical boundary layer latent heating is set to zero and where extratropical latent heating is decoupled throughout the vertical extent. The results are qualitatively similar, building confidence in the robustness of the experimental set-up and suggesting that latent heating in the free troposphere is more relevant than boundary layer latent heating for shaping the climatological circulation (not shown).

2.2. Data

Model outputs are stored on the native spatial model grid before being interpolated to 14 vertical pressure levels using logarithmic interpolation. We store the three-dimensional wind field, specific humidity, geopotential height, total diabatic temperature tendency (referred to as *diabatic heating*) and latent heating at 6-hourly time-steps.

2.2.1. Feature Tracking

We track cyclones using the TRACK algorithm (Hodges, 1994, 1995, 1999) on 850 hPa vorticity after applying a T42 truncation and removing spatial wave numbers smaller than or equal to 5. We only analyze features that persist longer than 2 days and travel further than 1,000 km. On the set of tracked cyclones, we compute the cyclone track density, genesis and lysis densities, cyclone propagation velocity, cyclone area and intensity for December, January, and February for each model year using spherical nonparametric estimators (Hodges, 1996).

Similar to Priestley et al. (2020), the track, genesis, and lysis densities are computed as the number of cyclones per month over an area equivalent to a 5° spherical cap, with genesis and lysis densities only considering the first and last time step of the cyclone track, respectively. The growth rate is in the units of day^{-1}, similar to the Eady growth rate and the intensity is taken as the maximum vorticity on 850 hPa during the cyclone lifetime. The cyclone area comprises the connected set of grid points defined by starting at the maximum 850 hPa vorticity in the cyclone and recursively searching for and connecting grid points of lower vorticity. In cases where the cyclones exist within two or more months, they are counted in the month they spend most of their lifetime.

2.2.2. Statistical Testing

To assess the statistical significance of the changes between the two experiments, we apply a two-sided Welch *t*-test on the monthly mean values of the data and the seasonal storm track statistics. We control the false discovery rate at a 0.05 level of significance to account for testing at multiple grid points (Wilks, 2016). The data points that reject the null hypothesis; that the expected value is the same, are referred to as "significant." For the tracked cyclones, grid points with less than two features per month per 5° spherical cap in either experiment are automatically labeled "insignificant."

3. Results

3.1. Decoupling Latent Heating From Wind and Temperature

The time mean latent heating on model levels is by construction identical in the control and the decoupled runs (not shown). For snapshots in time, however, the latent heating will be dramatically different (Figure 1). In the control run, which we will be referring to as the "coupled" run, latent heating is patchy, like the spatio-temporal distribution of clouds and precipitation. In the decoupled run, extratropical latent heating is fixed to a smooth and seasonally varying profile.

As a consequence of decoupling, the covariances between the full diabatic heating, meridional wind, and temperature dampen in the midlatitude free troposphere (Figure 2). The anomalies (asterisks) used to compute the covariances are deviations from the zonal mean (brackets). In the coupled run, diabatic heating is positively correlated with poleward wind and temperature in the free troposphere and negatively correlated close to the surface (Figures 2a and 2b). This is consistent with free troposphere latent heating in poleward warm air advection and sensible heating of colder air over warmer ocean at the surface. Prescribing free tropospheric latent heating reduces the amplitude of the full diabatic heating anomaly and thus largely reduces the covariances in the free troposphere (Figures 2c and 2d).

3.2. Coupling Enhances Eddy Heat Flux Efficiency

We have shown how decoupling latent heating changes the covariance of latent heating against wind and temperature. However, decoupling also changes the covariance of temperature and meridional wind (Figure 3d). In the following sections, to assess the effects of latent heating being coupled with the dynamics, we examine the differences between coupled and decoupled runs, where the latter is the baseline.

In the coupled run, the poleward lower tropospheric eddy heat flux $\left(\overline{v'T'}\right)$ increases in the North Atlantic and on the equatorward flanks of the North Pacific and Southern Hemispheric storm tracks compared to the decoupled run (Figure 3d). Simultaneously, the poleward eddy heat flux decreases over the continents and on the poleward flank of the North Pacific storm track. In this section, primes denote anomalies from a 10-day running mean (overbar).

The equatorward shift in eddy heat flux in the Southern Hemisphere and North Pacific can be explained by an equatorward shift in background baroclinicity ($|\overline{\theta}_y/\overline{\theta}_p|$; Figure 3a). We compute baroclinicity from 10-day running mean potential temperature $\left(\overline{\theta}\right)$ to represent the mean temperature gradient that the eddy heat fluxes interact with (Drouard et al., 2015).

We hypothesize that baroclinicity shifts equatorward in the coupled simulation due to realistic storm track latent heating typically occurring in the warm poleward moving air, east of troughs, on the warm side of the synoptic jets (Figure 3b; Auestad et al., 2024). While the heating occurs at relatively high latitudes it does so within air masses that, except when the synoptic wave breaks, are only temporally displaced poleward. Thus, baroclinicity is

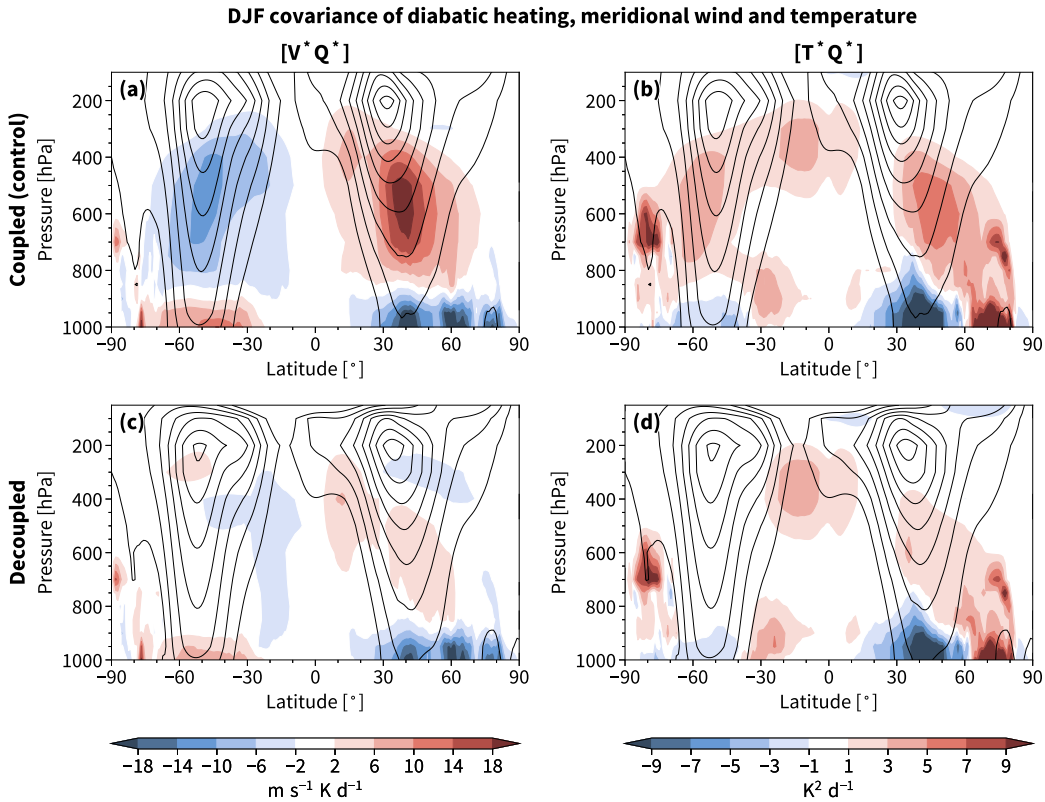

Figure 2. The covariance between the full diabatic heating (Q) and meridional wind (V; a and c, shading) in the coupled (a) and decoupled (c) runs. The covariance between full diabatic heating and temperature (T; b and d, shading) in the coupled (b) and the decoupled (d) runs. The zonal mean zonal wind is shown for reference in black contours with intervals $5, 10, \ldots, 50$ m s^{-1}. Values are averaged over December, January, and February.

maintained in relatively low-latitude air masses compared to the decoupled run, where baroclinicity is artificially increased at higher latitudes due to the unrealistic heating of cold, dry, high-latitude air masses by the prescribed latent heating (Figure 3c).

In the North Atlantic, however, the eddy heat flux increase is disproportionate to the changes in baroclinicity (Figures 3a and 3d). If the eddy heat flux were to be driven by a flux-gradient relationship, this would take the form

$$\overline{v'T'} = -\kappa \partial \overline{T}/\partial y, \tag{1}$$

where κ is an eddy diffusivity. The mean temperature gradient $\left(-\partial \overline{T}/\partial y\right)$ behaves similarly to our baroclinicity measure and thus, baroclinicity changes qualitatively explain the meridional dipole changes in eddy heat flux in the North Pacific and Southern Hemispheric storm tracks. In the North Atlantic, however, the increase in eddy heat flux does not follow the changes in baroclinicity.

To examine the changes in eddy character and diffusivity, we decompose the eddy heat flux into the product between the standard deviation of the meridional wind and temperature, and the correlation between the two,

$$\overline{v'T'} = \sigma_v \sigma_T corr(v, T). \tag{2}$$

The changes in eddy heat flux are further decomposed into linear contributions from changes in meridional wind, temperature, the correlation and a non-linear residual (R),

$$\Delta\overline{v'T'} = \sigma_v \sigma_T \Delta corr(v, T) + corr(v, T)\sigma_T \Delta\sigma_v + corr(v, T)\sigma_v \Delta\sigma_T + R. \tag{3}$$

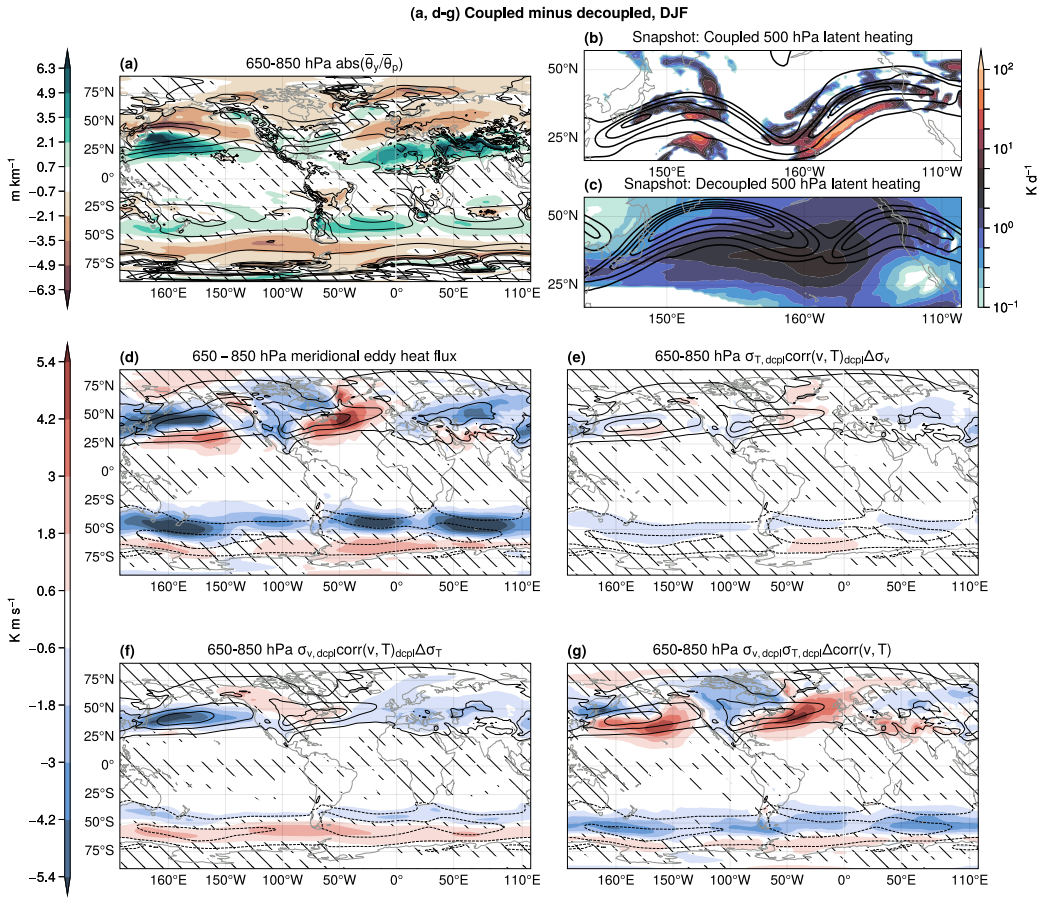

Figure 3. The coupled minus decoupled difference in 650–850 hPa baroclinicity (a), meridional eddy heat flux (d), and the linear contributions to the meridional eddy heat flux changes from changes in the meridional wind (e), the temperature (f), and the correlation between meridional wind and temperature (g). The black contours show the climatological values in the decoupled run, with intervals 5, 10, 15, 20 m km^{-1} (a) and ±3.5, 10.5, 17.5 K m s^{-1} (d–g). Values are averaged over December, January, and February and changes in the un-hatched grid points are significant (a, d–g). Panels (b, c) show 500 hPa latent heating (shading) and 300 hPa wind speed (contours; $40, 55, \ldots, 100$ m s^{-1}) for illustrative snapshots taken from February over the North Pacific.

Of these terms, the change in correlation explains most of the changes in the eddy heat flux from the decoupled to the coupled simulation (Figure 3g). In the North Pacific, North Atlantic, and Southern Hemispheric storm tracks the coupling between meridional wind and temperature is improved by realistic latent heating and eddies transport heat poleward more efficiently. Over the Northern hemispheric continents, in contrast, the correlation weakens and the poleward energy transport becomes less efficient.

The temperature anomalies mostly weaken in the coupled experiment, reducing the storm track eddy heat fluxes —largely consistent with the differences in baroclinicity (Figures 3a and 3f). Changes in the meridional wind (Figure 3e) are small and the residual is negligible (not shown), not contributing much to the eddy heat flux changes between the two experiments.

3.3. Coupling Causes Stronger and More Poleward Propagating Storms

In the storm tracks, the eddy heat flux is largely accomplished by cyclone growth and heat transport. Consistent with the changes in eddy heat flux, cyclones grow more intense when latent heating is coupled (Figure 4a).

Cyclone size also decreases in the main storm track regions in both hemispheres (Figure 4b). This is consistent with coupled latent heating leading to stronger but horizontally smaller regions of ascent (Booth et al., 2013; Emanuel et al., 1987; O'Gorman, 2011; Tierney et al., 2018). Simultaneously, cyclone size increases in the

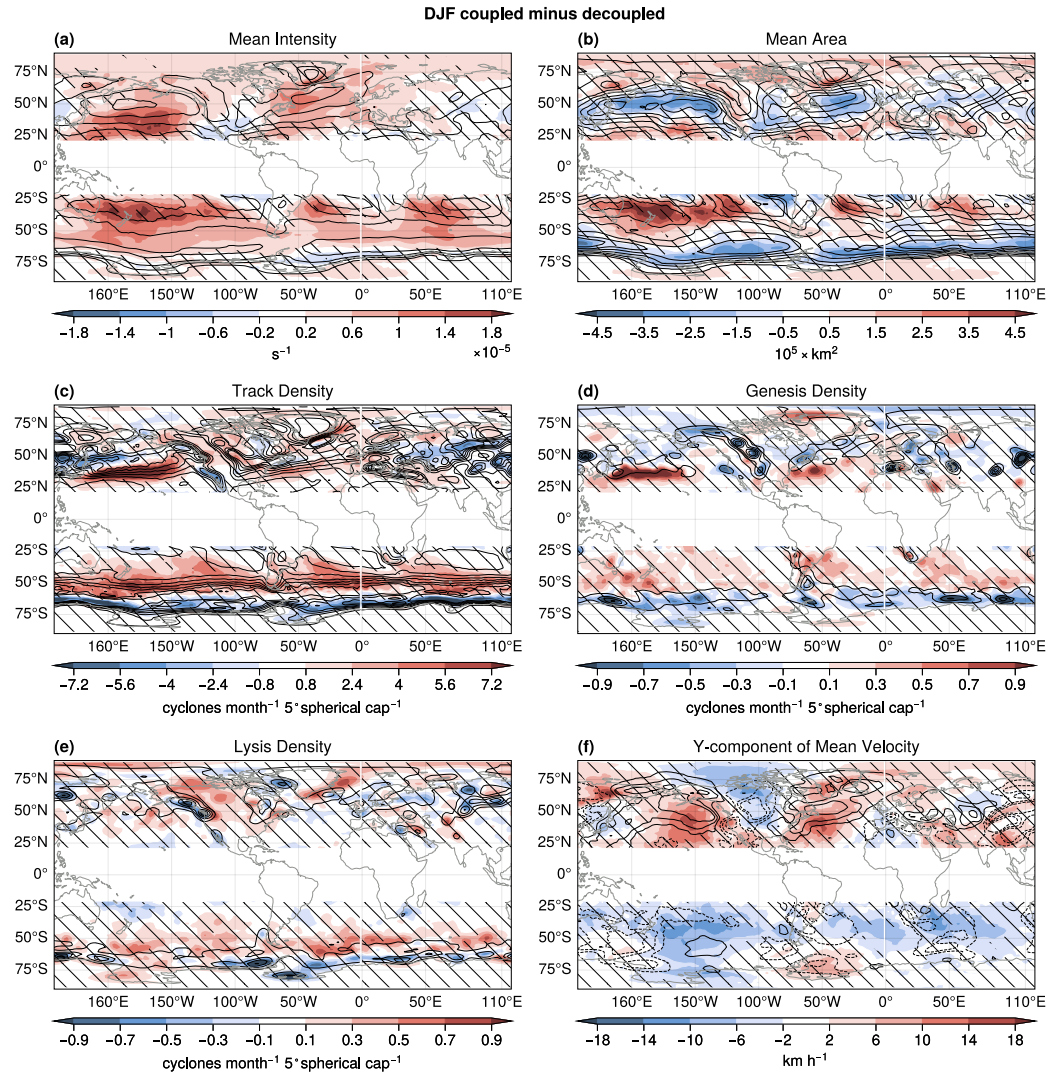

Figure 4. The coupled minus decoupled difference in cyclone intensity (a), cyclone area (b), track density (c), genesis density (d), lysis density (e), and mean meridional propagation velocity (f). The black contours show the climatological values in the decoupled run, with intervals 1, 2, 3, 4, 5 $\times 10^{-5}$ s^{-1} (a), 2.5, 5, 7.5, 10, 12.5, 15, 17.5 $\times 10^5$ km^2 (b), 1, 4, 8, 12, 16, 19 cyclones $month^{-1}$ 5 ° spherical cap^{-1} (c), 1, 2, 3, 4, 5 cyclones $month^{-1}$ 5 ° spherical cap^{-1} (d, e), and −15, −10, −5, 5, 10, 15 km h^{-1} (f). Values are from December, January, and February and changes in the un-hatched grid points are significant.

subtropics (significantly in the SH), which could reflect an equatorward shift of larger systems within the storm tracks.

Constituting an equatorward shift of the storm tracks, coupling increases the number of cyclones on the equatorward flank of the decoupled storm tracks—where also cyclogenesis increases (Figures 4c and 4d). In the North Atlantic and eastern North Pacific, where the climatological storm track is northeastward tilted, cyclolysis weakly increases around 60–70°N (Figure 4e).

Bridging the Northern Hemispheric increase in cyclogenesis (30–40°N) and lysis (60–70°N), the cyclones propagate more poleward in the climatologically tilted storm track regions when latent heating is coupled (Figure 4f). Cyclones also propagate more poleward in the Southern Hemisphere when latent heating is coupled, but less regionally confined and in a more zonally symmetric fashion compared to the Northern Hemisphere.

The enhanced poleward propagation is consistent with the effect of latent heating on lower tropospheric PV relative to the cyclone core and the general increase in cyclone growth rate with coupled latent heating

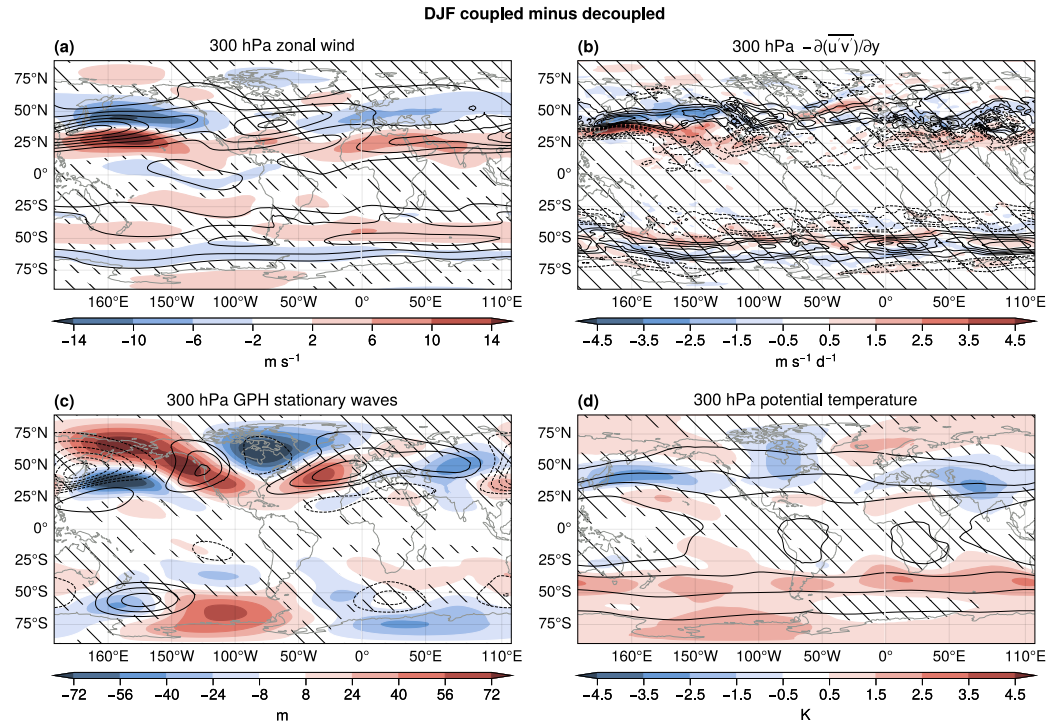

Figure 5. The coupled minus decoupled difference in 300 hPa zonal wind (a), 300 hPa meridional eddy momentum flux convergence (b), 300 hPa geopotential height stationary waves (c), and 300 hPa potential temperature (d). Climatological values in the decoupled run are shown in black in contours with intervals 10, 20, …, 60 m s^{-1} (a), ±1, 2, …, 5 m s^{-1} d^{-1} (b), ±50, 100, …, 300 m (c), and 310, 320, 330, 340 *K* (d). Values are averaged over December, January, and February and changes in the un-hatched grid points are significant.

(Tamarin & Kaspi, 2016). The equatorward shift of the storm tracks, primarily the North Pacific and the Southern Hemispheric storm tracks shift equatorward, is less intuitive and discussed next.

3.4. Coupling Shifts the Mean Jet Equatorward and 'Splits' It

Like the storm tracks, the time mean jet shifts equatorward in the North Pacific and Southern Hemisphere when latent heating is coupled (Figure 5a). The signal is not limited to the storm tracks but is largely zonally symmetric and visible throughout the vertical extent of the troposphere (not shown).

The equatorward jet shift likely follows the coupling-induced equatorward shift in baroclinicity, discussed in Section 3.2: latent heating in the subtropical air maintains baroclinicity, and thus a jet, at lower latitudes (Figure 3a). Consistently, cyclogenesis increases at lower latitudes in the coupled run (Figure 4d) and the transient meridional eddy momentum flux convergence shifts equatorward with the jet, indicating more poleward eddy propagation from the lower genesis latitudes, leaving a stronger time mean subtropical jet (Figure 5b).

With coupled latent heating, a tendency for "split jets" emerges over the North Atlantic and the eastern North Pacific. In these regions, the storm track tilt is enhanced by coupled latent heating (Figure 4f). The split jet tendency features reduced westerlies around 45°N and enhanced westerlies further poleward, further tilting the time mean jet. The reduced westerlies could also indicate more or stronger blocking events, consistent with the latent heating effect on blocks (Pfahl et al., 2015).

Via its non-linear relationship with the dynamics, the transient latent heating shapes the time mean zonally asymmetric circulation as expressed by stationary waves. The stationary waves are computed as anomalies in monthly mean geopotential height from the zonal average ($\overline{z}^* = \overline{z} - [\overline{z}]$). The equatorward jet shift in the western North Pacific manifests as a meridional shift in the stationary wave pattern (Figure 5c). The enhanced poleward propagation of storms and "split-jet" tendency in the eastern North Pacific and North Atlantic projects onto the stationary wave pattern by amplifying the ridges there and the trough over North America.

We finally note that our results are robust to the method of decoupling. Solomon (2006) decoupled latent heating by redistributing the heating over zonal bands. The experiment of Solomon (2006) shows that coupling latent heating enhances eddy heat fluxes, causing an upper-tropospheric polar amplification in the Northern Hemisphere and generally warmer upper-tropospheric temperatures in the Southern Hemisphere in December-February, similar to our results (Figures 3d and 5d). The upper-tropospheric warming results from ascending air parcels following the moist adiabatic lapse rate in the coupled run, which increases mean static stability (not shown; Juckes, 2000). The Supporting Information S1 contains June, July, and August versions of Figures 2–5.

4. Summary and Discussion

Latent heating within the storm tracks feeds back on the circulation over a range of spatio-temporal scales. Here, we demonstrate the climatological latent heating feedback effect in an atmosphere-only model (CAM4) by comparing a run with realistic latent heating (coupled experiment) against a run with latent heating prescribed in the extratropics (decoupled experiment).

To decouple, real-time latent heating is replaced by the climatological monthly mean latent heating in the coupled experiment, such that the time-mean extratropical latent heating in the two runs is identical, while allowing for transient differences (Figures 1, 3b, and 3c). The non-linear relationship between latent heating and circulation causes significant differences in the extratropical mean jet and storm track characteristics between the two runs.

Coupling latent heating leads to an equatorward shift in the midlatitude baroclinicity, thus also shifting the eddy heat flux in the North Pacific and the Southern Hemisphere equatorward (Figures 3a and 3d). In the North Atlantic, however, eddy heat fluxes increase disproportionately to baroclinicity as a result of eddies transporting heat poleward more efficiently in the coupled- compared to the decoupled simulation (Figure 3g).

Cyclones grow more intense in the coupled run compared to the decoupled run (Figure 4a), consistent with how latent heating increases PV below the heating maximum and enhances ascent within the cyclone (e.g., Wernli & Gray, 2023). Where the subtropical jet is weak, cyclones also propagate more poleward in the coupled run (Figure 4f), contributing to the zonally asymmetric state (Figure 5c; Schemm, 2023; Tamarin & Kaspi, 2016).

The subtropical jets strengthen in the coupled run compared to the decoupled run, a signal which is largely zonally symmetric (Figure 5a). To explain this, we suggest that since realistic latent heating occurs in poleward moving warm airmasses (Figure 2; Auestad et al., 2024) that often will return to lower latitudes, baroclinicity is maintained at lower latitudes in the coupled run, compared to the decoupled run. In the decoupled run, latent heating also occurs in the cold and equatorward-moving air, artificially forcing baroclinicity and therefore the jet at higher latitudes (Section 3.2).

As the hydrological cycle amplifies in a warming world, so will latent heating. There are large uncertainties as to how jets and storm tracks respond to increasing greenhouse gas concentrations and the physical drivers are hard to isolate due to the nonlinearities (Ossó et al., 2024). In a follow-up study, we will examine the latent heating feedback in a climate change scenario assessing its effect on the jet stream and storm track aiming to disentangle the contributions from the mean and transient latent heating as the atmosphere warms.

Acknowledgments
We would like to thank Kevin Hodges for providing and helping with the cyclone tracking algorithm, Paul O'Gorman and Tiffany Shaw for useful discussions, and the two anonymous reviewers for their constructive comments. HA acknowledges Aker Scholarship and Laanekassen. PC was supported by UK Natural Environmental Research Council Grants NE/V012045/1 and NE/T006250/1. PC and AS were supported by UK Research and Innovation (UKRI) under the UK government's Horizon Europe funding Guarantee (Grant EP/Y036123/1). This work used the ARCHER2 UK National Supercomputing Service (https://www.archer2.ac.uk).

Data Availability Statement

CAM4 is described by Neale et al. (2010) and available via https://github.com/ESCOMP/CESM (ESCOMP, 2025).

References

Auestad, H., Spensberger, C., Marcheggiani, A., Ceppi, P., Spengler, T., & Woollings, T. (2024). Spatio-temporal averaging of jets obscures the reinforcement of baroclinicity by latent heating. *Weather and Climate Dynamics*, *5*(4), 1269–1286. https://doi.org/10.5194/wcd-5-1269-2024

Beckett, G., Beech-Brandt, J., Leach, K., Payne, Z., Simpson, A., Smith, L., et al. (2024). ARCHER2 service description (technical report). *Zenodo*. https://doi.org/10.5281/zenodo.14507040

Booth, J. F., Wang, S., & Polvani, L. (2013). Midlatitude storms in a moister world: Lessons from idealized baroclinic life cycle experiments. *Climate Dynamics*, *41*(3), 787–802. https://doi.org/10.1007/s00382-012-1472-3

Bukenberger, M., Rüdisühli, S., & Schemm, S. (2023). Jet stream dynamics from a potential vorticity gradient perspective: The method and its application to a kilometre-scale simulation. *Quarterly Journal of the Royal Meteorological Society*, *149*(755), 2409–2432. https://doi.org/10.1002/qj.4513

Drouard, M., Rivière, G., & Arbogast, P. (2015). The link between the North Pacific climate variability and the North Atlantic oscillation via downstream propagation of synoptic waves. *Journal of Climate*, *28*(10), 3957–3976. https://doi.org/10.1175/JCLI-D-14-00552.1

Duchon, C. E. (1979). Lanczos filtering in one and two dimensions. *Journal of Applied Meteorology and Climatology*, *18*(8), 1016–1022. https://doi.org/10.1175/1520-0450(1979)018⟨1016:LFIOAT⟩2.0.CO;2

Emanuel, K. A., Fantini, M., & Thorpe, A. J. (1987). Baroclinic instability in an environment of small stability to slantwise moist convection. Part I: Two-dimensional models. *Journal of the Atmospheric Sciences*, *44*(12), 1559–1573. https://doi.org/10.1175/1520-0469(1987)044⟨1559:BIIAEO⟩2.0.CO;2

ESCOMP. (2025). CESM [Software]. Earth System Community Modeling Portal.

Hack, J. J. (1994). Parameterization of moist convection in the National Center for Atmospheric Research community climate model (CCM2). *Journal of Geophysical Research*, *99*(D3), 5551–5568. https://doi.org/10.1029/93JD03478

Harvey, B., Methven, J., Sanchez, C., & Schäfler, A. (2020). Diabatic generation of negative potential vorticity and its impact on the North Atlantic jet stream. *Quarterly Journal of the Royal Meteorological Society*, *146*(728), 1477–1497. https://doi.org/10.1002/qj.3747

Held, I. M., Ting, M., & Wang, H. (2002). Northern winter stationary waves: Theory and modeling. *Journal of Climate*, *15*(16), 2125–2144. https://doi.org/10.1175/1520-0442(2002)015⟨2125:NWSWTA⟩2.0.CO;2

Hermoso, A., Rivière, G., Harvey, B., Methven, J., & Schemm, S. (2024). A dynamical interpretation of the intensification of the winter north Atlantic jet stream in reanalysis. *Journal of Climate*, *37*(22), 5853–5881. https://doi.org/10.1175/JCLI-D-23-0757.1

Hodges, K. I. (1994). A general method for tracking analysis and its application to meteorological data. *Monthly Weather Review*, *122*(11), 2573–2586. https://doi.org/10.1175/1520-0493(1994)122⟨2573:AGMFTA⟩2.0.CO;2

Hodges, K. I. (1995). Feature tracking on the unit sphere. *Monthly Weather Review*, *123*(12), 3458–3465. https://doi.org/10.1175/1520-0493(1995)123⟨3458:FTOTUS⟩2.0.CO;2

Hodges, K. I. (1996). Spherical nonparametric estimators applied to the UGAMP model integration for AMIP. *Monthly Weather Review*, *124*(12), 2914–2932. https://doi.org/10.1175/1520-0493(1996)124⟨2914:SNEATT⟩2.0.CO;2

Hodges, K. I. (1999). Adaptive constraints for feature tracking. *Monthly Weather Review*, *127*(6), 1362–1373. https://doi.org/10.1175/1520-0493(1999)127⟨1362:ACFFT⟩2.0.CO;2

Hoskins, B. J., & Valdes, P. J. (1990). On the existence of storm tracks. *Journal of the Atmospheric Sciences*, *47*(15), 1854–1864. https://doi.org/10.1175/1520-0469(1990)047<1854:oteost>2.0.co;2

Hurrell, J. W., Hack, J. J., Shea, D., Caron, J. M., & Rosinski, J. (2008). A new sea surface temperature and sea ice boundary dataset for the community atmosphere model. *Journal of Climate*, *21*(19), 5145–5153. https://doi.org/10.1175/2008JCLI2292.1

Juckes, M. N. (2000). The static stability of the midlatitude troposphere: The relevance of moisture. *Journal of the Atmospheric Sciences*, *57*(18), 3050–3057. https://doi.org/10.1175/1520-0469(2000)057⟨3050:TSSOTM⟩2.0.CO;2

Kaspi, Y., & Schneider, T. (2013). The role of stationary eddies in shaping midlatitude storm tracks. *Journal of the Atmospheric Sciences*, *70*(8), 2596–2613. https://doi.org/10.1175/JAS-D-12-082.1

Lachmy, O., & Kaspi, Y. (2020). The role of diabatic heating in ferrel cell dynamics. *Geophysical Research Letters*, *47*(23), e2020GL090619. https://doi.org/10.1029/2020GL090619

Laîné, A., Lapeyre, G., & Rivière, G. (2011). A quasigeostrophic model for moist storm tracks. *Journal of the Atmospheric Sciences*, *68*(6), 1306–1322. https://doi.org/10.1175/2011JAS3618.1

Madonna, E., Limbach, S., Aebi, C., Joos, H., Wernli, H., & Martius, O. (2014). On the co-occurrence of warm conveyor belt outflows and PV streamers. *Journal of the Atmospheric Sciences*, *71*(10), 3668–3673. https://doi.org/10.1175/JAS-D-14-0119.1

Madonna, E., Wernli, H., Joos, H., & Martius, O. (2014). Warm conveyor belts in the ERA-interim dataset (1979–2010). Part I: Climatology and potential vorticity evolution. *Journal of Climate*, *27*(1), 3–26. https://doi.org/10.1175/JCLI-D-12-00720.1

Methven, J. (2015). Potential vorticity in warm conveyor belt outflow. *Quarterly Journal of the Royal Meteorological Society*, *141*(689), 1065–1071. https://doi.org/10.1002/qj.2393

Neale, R. B., Richter, J., Park, S., Lauritzen, P. H., Vavrus, S. J., Rasch, P. J., & Zhang, M. (2013). The mean climate of the community atmosphere model (CAM4) in forced SST and fully coupled experiments. *Journal of Climate*, *26*(14), 5150–5168. https://doi.org/10.1175/JCLI-D-12-00236.1

Neale, R. B., Richter, J. H., Conley, A. J., Park, S., Lauritzen, P. H., Gettelman, A., et al. (2010). Description of the NCAR community atmosphere model (CAM 4.0).

O'Gorman, P. A. (2011). The effective static stability experienced by eddies in a moist atmosphere. *Journal of the Atmospheric Sciences*, *68*(1), 75–90. https://doi.org/10.1175/2010JAS3537.1

Ossó, A., Bladé, I., Karpechko, A., Li, C., Maraun, D., Romppainen-Martius, O., et al. (2024). Advancing our understanding of Eddy-driven jet stream responses to climate change—A roadmap. *Current Climate Change Reports*, *11*(1), 2. https://doi.org/10.1007/s40641-024-00199-3

Papritz, L., & Spengler, T. (2015). Analysis of the slope of isentropic surfaces and its tendencies over the North Atlantic. *Quarterly Journal of the Royal Meteorological Society*, *141*(693), 3226–3238. https://doi.org/10.1002/qj.2605

Pauluis, O., Czaja, A., & Korty, R. (2010). The global atmospheric circulation in moist isentropic coordinates. *Journal of Climate*, *23*(11), 3077–3093. https://doi.org/10.1175/2009JCLI2789.1

Pfahl, S., Schwierz, C., Croci-Maspoli, M., Grams, C. M., & Wernli, H. (2015). Importance of latent heat release in ascending air streams for atmospheric blocking. *Nature Geoscience*, *8*(8), 610–614. https://doi.org/10.1038/ngeo2487

Priestley, M. D. K., Ackerley, D., Catto, J. L., Hodges, K. I., McDonald, R. E., & Lee, R. W. (2020). An overview of the extratropical storm tracks in CMIP6 historical simulations. *Journal of Climate*, *33*(15), 6315–6343. https://doi.org/10.1175/JCLI-D-19-0928.1

Rasch, P. J., & Kristjánsson, J. E. (1998). A comparison of the CCM3 model climate using diagnosed and predicted condensate parameterizations. *Journal of Climate*, *11*(7), 1587–1614. https://doi.org/10.1175/1520-0442(1998)011⟨1587:ACOTCM⟩2.0.CO;2

Schemm, S. (2023). Toward eliminating the decades-old "Too Zonal and Too Equatorward" storm-track bias in climate models. *Journal of Advances in Modeling Earth Systems*, *15*(2), e2022MS003482. https://doi.org/10.1029/2022MS003482

Solomon, A. (2006). Impact of latent heat release on polar climate. *Geophysical Research Letters*, *33*(7), L07716. https://doi.org/10.1029/2005GL025607

Tamarin, T., & Kaspi, Y. (2016). The poleward motion of extratropical cyclones from a potential vorticity tendency analysis. *Journal of the Atmospheric Sciences*, *73*(4), 1687–1707. https://doi.org/10.1175/JAS-D-15-0168.1

Tierney, G., Posselt, D. J., & Booth, J. F. (2018). An examination of extratropical cyclone response to changes in baroclinicity and temperature in an idealized environment. *Climate Dynamics*, *51*(9), 3829–3846. https://doi.org/10.1007/s00382-018-4115-5

Wernli, H., & Gray, S. L. (2023). The importance of diabatic processes for the dynamics of synoptic-scale extratropical weather systems—A review (preprint). *Dynamical processes in midlatitudes*. https://doi.org/10.5194/egusphere-2023-2678

White, I. P., Lachmy, O., & Harnik, N. (2024). Influence of a local diabatic heating source on the midlatitude circulation. *Quarterly Journal of the Royal Meteorological Society*, *150*(765), 5167–5187. https://doi.org/10.1002/qj.4863

Wilks, D. S. (2016). "The stippling shows statistically significant grid points": How research results are routinely overstated and overinterpreted, and what to do about it. *Bulletin of the American Meteorological Society*, *97*(12), 2263–2273. https://doi.org/10.1175/BAMS-D-15-00267.1

Woollings, T., Papritz, L., Mbengue, C., & Spengler, T. (2016). Diabatic heating and jet stream shifts: A case study of the 2010 negative North Atlantic Oscillation winter. *Geophysical Research Letters*, *43*(18), 9994–10002. https://doi.org/10.1002/2016GL070146

Xia, X., & Chang, E. K. M. (2014). Diabatic damping of zonal index variations. *Journal of the Atmospheric Sciences*, *71*(8), 3090–3105. https://doi.org/10.1175/JAS-D-13-0292.1

Zhang, G., & McFarlane, N. A. (1995). Sensitivity of climate simulations to the parameterization of cumulus convection in the Canadian climate centre general circulation model. *Atmosphere-Ocean*, *33*(3), 407–446. https://doi.org/10.1080/07055900.1995.9649539

Zhang, G., & Wang, Z. (2018). North Atlantic extratropical Rossby wave breaking during the warm season: Wave life cycle and role of diabatic heating. *Monthly Weather Review*, *146*(3), 695–712. https://doi.org/10.1175/MWR-D-17-0204.1